[1.]M.A. BODUDE, [2.]R.N. NNAJI, [3.]L.O. OSOBA

COMPARATIVE STUDIES ON THE HIGH TEMPERATURE OXIDATION BEHAVIOUR OF HAYNES 282 AND INCONEL 718 NICKEL–BASED SUPERALLOYS

[1–3.]Department of Metallurgical and Materials Engineering, University of Lagos, Akoka, Lagos, NIGERIA

Abstract: Nickel–based superalloys are heat–resistant metallic materials used in the fabrication of hot–section components of aero– and land–based gas turbine engines. At high temperatures in oxidizing environments, gas turbine superalloy components depend on the formation of stable, compact, and adherent oxide layers on their surfaces for protection against high temperature oxidation. However, at temperatures above 1000°C, certain protective oxides become volatile, thereby limiting the protective properties of such oxides. In this present investigation, the high temperature oxidation behaviour of Haynes 282 and Inconel 718 nickel–based superalloys were examined under isothermal conditions through gravimetric experimental study, microscopic observation of the morphology of the surface oxides formed, and elemental composition of the formed–oxides at 1050 °C and 1100°C for a maximum exposure period of 10 hours. The morphology and elemental compositions of the surface oxides formed after the oxidation experiments were assessed using Scanning Electron Microscopy (SEM) and X–ray Energy Dispersive Spectroscopy (EDS). The isothermal oxidation rate constant, kp was calculated from the gravimetric data analysis for the superalloys at both test temperatures and found to be kp = 1.87 (mg^2/cm^4. h) and 8.24 (mg^2/cm^4. h) for Haynes 282; and kp = 0.49 (mg^2/cm^4. h) and 7.70 (mg^2/cm^4. h) for Inconel 718 at 1050 and 1100 °C test temperatures respectively. Haynes 282 had an overall higher weight gain and higher kp than Inconel 718 at both test temperatures as obtained from the oxidation kinetics. After 10 hours' exposure at 1050°C and 1100°C, the surface SEM image of Haynes 282 specimen showed crystal–like oxides structures, while Inconel 718 showed amorphous oxide clusters with pores. EDS results suggested presence of titanium and chromium oxides for Haynes 282 and predominantly chromium oxide for Inconel 718.

Keywords: Haynes 282, Inconel 718, Oxidation kinetics, Oxides, Superalloys

INTRODUCTION

Superalloys are heat–resistant multi–component metallic materials designed for high temperature applications such as jet engines and power–generation gas turbines. Intensive superalloy development and processing over the past few decades have resulted in nickel–based superalloys that can tolerate average temperatures of 1050°C with occasional short trips (near airfoil tips) to temperatures as high as 1200°C. The popularity of nickel–based superalloys in high–temperature applications is largely due to their high–temperature oxidation and creep resistance (Pérez–González *et al*., 2014; Pollock and Tin, 2006; Wu *et al*., 2010). Superalloys premier introduction into military gas turbine engines in the second quarter of the 20th century (during World War II) led to significant improvement in jet engine production technology in the modern aerospace industry (Barbosa *et al*., 2005). The largest application of superalloys is in the gas turbine industry, where good mechanical strength and thermal stability at service temperatures are required (Shukla *et al*., 2013).

Improved efficiency is the requirement for all types of modern gas turbines and this often happens with increase in operating temperature, which also increases the risk of high–temperature oxidation in the material components. Gas turbine blades are one of the most critical aircraft engine components affected by high–temperature oxidation. For best performance of the engine, the combustion temperature should be the maximum obtainable from the complete combustion of the oxygen and the fuel (Eliaz *et al*., 2002). The total power produced as well as the engine efficiency often depend on the condition of individual turbine blade. In attempts to generate more power with improved efficiency, gas turbine engines have steadily become bigger and more sophisticated over the past twenty years. Therefore, the turbine blades must also be capable of operating in more demanding environments. These environments typically include but not limited to high centrifugal stresses and very high temperatures (surpassing 1500°C), which lead to fast degradation of the turbine blades and ultimately weakens overall engine performance through mechanisms such as high–temperature oxidation (Saravanamutto *et al*., 2009; Caron and Khan, 1999; Smith, 2013).

At temperatures above 1000°C high–temperature oxidation becomes a very significant problem and most nickel–based superalloys are used at such temperatures in service. Above this temperature, the oxidation resistance of gas turbine superalloy components reduces rapidly (Mahobia *et al*., 2013; Zitnansky *et al*., 1998). The service environment of the gas turbine is highly oxidizing; therefore, hot–gas–path components depend on formation of compact oxide layers to provide protection against high–temperature oxidation. However, a stable and protective oxide may crack, spall or even form volatile compounds above a certain temperature point under high–temperature exposures leading to loss in oxidation resistance (Ahlatci, 1991). For instance, the rate of formation of chromium oxides is quick in comparison with aluminium oxides. Therefore, chromium oxide is often

preferred to aluminium oxide given that it will form quickly to protect the base material, and will also repair itself quickly if the oxide layer spalls or becomes damaged by foreign object fragments. However, chromium oxide becomes volatile at temperatures above 1000°C, therefore requiring the formation of more stable oxides, like aluminium oxide, for operating temperatures exceeding 1000°C (ASM, 1997; Pomeroy, 2005; Smith, 2013).

Regardless of the advancements in superalloy compositions and microstructure through manufacturing processes, working temperatures in excess of 70–90% melting temperature of the material are pushing the limits of even the most resilient superalloys. Due to the presence of several alloying elements in superalloys (as many as 10 to 15 different elements or more), their reactions with different environments encountered in practice can result in rather complex processes. Superalloys are classified into three main groups namely, iron–based, cobalt–based, and nickel–based (Pollock and Tin, 2006; Pérez–González *et al*., 2014; Barbosa *et al*., 2005).

MATERIALS AND METHODS

Rectangular specimens were prepared from as–received bars of Haynes 282 and Inconel 718 superalloys. Each sample of both Haynes 282 and Inconel 718 superalloys was cut to an approximate dimension of 1.06 cm x 0.8 cm x 0.4 cm (length x width x thickness). Samples were ground using 600, 800, and 1,200 grit in succession (to remove all surface oxides). The samples were then cleaned by immersing them in methylated spirit for 10 minutes and thereafter, washed with hot water to remove any possible oil or residue contaminants deposited on the sample during the cutting and grinding processes.

Samples in this set were prepared following the procedure outlined in Section 3.1 for isothermal oxidation test at 1050°C. Samples and the crucibles were weighed before the oxidation experiments using a digital weighing scale (Shimadzu UW1020H) sensitive to 0.001g. Afterwards, the samples were placed in specific arrangements in the crucibles and then on a stainless–steel plate (secondary plate) and held in place by a mild steel plate (primary plate) as shown in Plates 3(a) and (b) and, subsequently placed inside the furnace. The samples were placed in the furnace at ambient temperatures and heating continued until the furnace temperature stabilized at 1050°C.

The samples and crucibles were oxidized at 1050°C for different exposure times ranging from 4 to 10 hours for either of both superalloys. Upon removal from the furnace, the oxidized weights of the samples and crucibles were taken using the same digital scale as above and weight gain was calculated. The oxidized samples after the weight gain calculations were wrapped in aluminium foil and labelled accordingly for further analyses.

Oxidation tests at 1100°C for Haynes 282 and Inconel 718 superalloy samples followed the same procedure above as described for the 1050°C test temperature.

Samples used in this work were created from the same as–received Haynes 282 and Inconel 718 superalloy bars respectively. Rectangular specimens were prepared from as–received bars of of 1.06 cm x 0.8 cm x 0.4 cm for both Haynes 282 and Inconel 718 superalloys. Each sample were placed in specific arrangements in the crucibles and then on a stainless steel plate (secondary plate) and held in place by a mild steel plate (primary plate) as shown in Figure 1(a) and, subsequently placed inside the furnace. The arrangement had Haynes 282 alloy samples on the left side of the plate and Inconel 718 alloy samples on the right side inside the furnace [Figure 1(b)].

(a)

(b)

(c)

(d)

Figure 1. Experimental Setup: (a) sample arrangement inside the crucible; (b) crucible arrangement in the furnace; (c) furnace stability at first test temperature; (d) furnace environment before samples were retrieved

The samples and crucibles were oxidized at 1050°C for different exposure times between 4 to 10 hours for either of both superalloys [Figure 1 (c)]. Upon removal from the

furnace [Figure 1 (d)], the oxidized weights of the samples and crucibles were taken using the same digital scale as above and weight gain was calculated. Oxidation tests at 1100°C for both superalloy samples followed the same procedure outlined above.

— Light Optical Microscopy (LOM)

The test samples were carefully sectioned along their lengths using a fresh hardened–steel hack–saw blade one at a time for each sample and the cross sections were mounted in epoxy (resin). Sample surface grinding was conducted with successive finer wet silicon carbide papers from 220 to 1200 grit. The edges were properly chamfered and rounded to ensure a proper flat surface of the specimens during the grinding operations.

The samples were then polished using 0.3 µm and 0.05 µm alumina slurries sequentially. The samples were properly washed under running water and dried using hot air. Samples were chemically etched and once again properly washed under running water and dried using hot air. The longitudinal cross–sectional areas of the oxidized specimens were examined using light optical microscope type [CETI] fitted with digital camera (5 Mega Pixels resolution) in the Laboratory at the Department of Metallurgical and Materials Engineering, University of Lagos.

Samples of the as–received Haynes 282 and Inconel 718 superalloys were also subjected to the above metallographic procedures and etched for Light Optical Microscopy. To visualize the thickness of the oxide film, optical micrographs of the boundaries between the oxidized specimens' cross–sections and the epoxy were taken.

— Scanning Electron Microscopy (SEM) and Energy Dispersive X–ray Spectroscopy (EDS)

To further examine the morphology and composition of the surface oxides formed, SEM (Scanning Electron Microscopy) and EDS (X–ray Energy Dispersive Spectroscopy) were used. EDS was used to identify the elemental composition of the oxides on the surface of the samples. For this investigation, the Phenom Desktop SEM machine with Phenom ProX software attached, in Covenant University, Ota, Ogun State, Nigeria was used.

RESULTS AND DISCUSSION

— Results

The average nominal compositions of the as–received Haynes 282 and Inconel 718 superalloys given by the PMI (Positive Material Identification) machine at Midwal Engineering and Testing Laboratory, Lekki, Lagos, Nigeria are shown in Table 1.

Table 1: Average Nominal Composition of As–Received Haynes 282 and Inconel 718 Superalloys (wt. %)

Element	Ni	Cr	Fe	Nb	Mo	Ti	Al
Haynes 282	57.96	18.03	2.81	–	8.62	1.97	ND
Inconel 718	50.08	18.98	18.95	5.03	3.14	1.00	ND
Element	Co	C	Mn	Si	P	S	B	Cu
Haynes 282	9.40	ND	0.13	ND	–	–	–	ND
Inconel 718	0.24	ND	0.09	ND	ND	ND	ND	ND

ND = Not Determined

Three locations on each alloy sample were x–rayed using the PMI machine and the averages were calculated as shown in the table.

— Oxidation Performance and Weight Change

The entire surface area was used for the calculation of the weight change per area, which was approximately 0.85 cm^2 for both superalloy test samples. Most of the oxidation observed took place on the top surface exposed to the oxidizing environment as shown in the sample arrangement in Plate 3(a) and therefore, contributed the most to the weight gain of each sample (Olivares *et al.*, 2013; Smith, 2013). Observations from the weight change measurements show that both superalloy samples gained weight at both test temperatures at all oxidation times except for Haynes 282 sample oxidized for 4 hours at 1050°C.

Haynes 282 had a sharp weight gain between 4–6 hours' exposure–time at 1050°C, followed by a drop–in weight gain between the 6–8 hours' exposure–time. However, there was further gain in weight between the 8–10 hours' exposure–time. Inconel 718 superalloy displayed a steady increase in weight gain between the 4–8 hours' exposure–time. There was a drop–in weight gain between the 8–10 hours' exposure time at 1050°C.

Similarly, the weight gain calculations and plot for both superalloys at the 1100°C test temperature are shown in Table 5 (A and B) and Figure 5 respectively.

At 1100°C, Haynes 282 showed an almost linear increase in weight gained by the samples across the length of the exposure time. Inconel 718 showed increase in weight gained by the samples between 4–8 hours' exposure–time, with equal weight gain at 8 and 10 hours exposure time (Figure 5). Weight change during an isothermal oxidation process has been reported to follow a relationship of the form:

$$\Delta W = k_p \times t^{0.5} \quad (1)$$

where, ΔW represents the weight gain per unit area in mg/cm^2, k_p the isothermal oxidation rate constant in $mg^2\ cm^{-4}\ h^{-1}$, and t is the oxidation time at a particular temperature in hours. Equation (1) implies that weight gain, (ΔW), is proportional to the square root of time ($t^{0.5}$). (Pérez–González et al., 2014; Olivares et al., 2013; Sinharoy and Narasimhan, 2004).

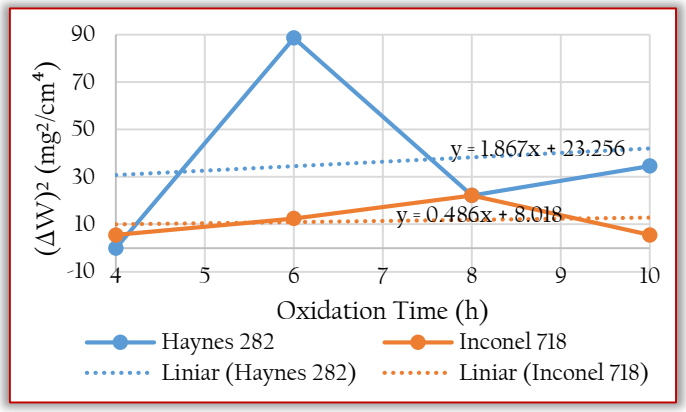

Figure 2. Isothermal rate constant for oxidation of Haynes 282 and Inconel 718 superalloys at 1050°C

By approximating the oxidation kinetics to Equation (9), a plot of the square of weight gain versus time ($\Delta W^2 = k_p x\ t$, allows for the estimation of the isothermal oxidation rate constant, k_p (Olivares et al., 2013).

By plotting the square of weight gain versus time and ignoring scatter, an overall isothermal oxidation rate constant, k_p, is approximately determined from the slope of the best–fit straight line as shown in Figures 2 and 3 for 1050 and 1100°C test temperatures respectively.

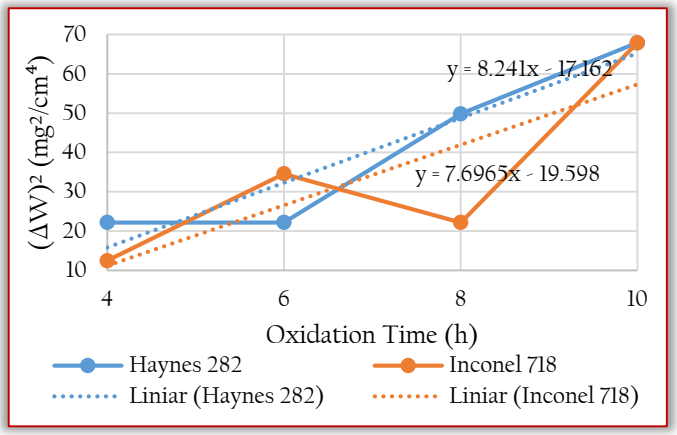

Figure 3. Isothermal rate constant for oxidation of Haynes 282 and Inconel 718 superalloys at 1100°C

— Summary of Oxidation Tests

Weight gain as well as the isothermal oxidation rate was observed to increase with temperature for both Haynes 282 and Inconel 718 at the 1050 and 1100°C test temperatures. The oxidation rate constant of Haynes 282, the slope of the fitted straight line, is about 3.8 times higher (1.87 mg^2/cm^4. h) than that of Inconel 718 (0.49 mg^2/cm^4. h) at 1050°C.

At 1100°C, the oxidation rate of Haynes 282, the slope of the best–fit straight line, is approximately 1.1 times more (8.24 mg^2/cm^4. h) than that of Inconel 718 (7.70 mg^2/cm^4. h).

Table 2: Summary of high temperature oxidation of Haynes 282 and Inconel 718 superalloys at 1050 and 1100 °C test temperatures

Alloy type	1050°C		1100°C	
	Total wt. gain, 10 h (mg/cm^2)	Isothermal oxidation rate (mg^2/cm^4 . h)	Total wt. gain, 10 h (mg/cm^2)	Isothermal oxidation rate (mg^2/cm^4 . h)
Haynes 282	20.00	1.87	24.72	8.24
Inconel 718	12.94	0.49	22.36	7.70

— Light Optical Microstructural Analysis

Light optical microstructural analysis of cross–sections of the oxidized samples of both superalloys was carried out in an attempt to determine the thickness of the formed–surface–oxides (Plates 2–9).

The micrographs were observed at the boundary between the epoxy mount and the samples cross sections at 100x magnification. Microstructure of the as–received superalloy samples were also examined (Plate 1 a, and b).

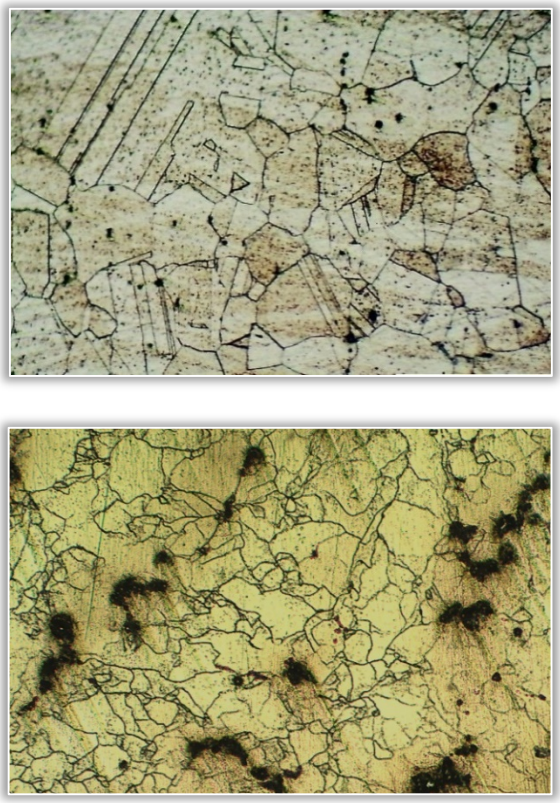

(a) (b)

Plate 1. Optical micrographs of (a) As–Received Haynes 282 (100*x*), (b) As–Received Inconel 718 (100*x*)

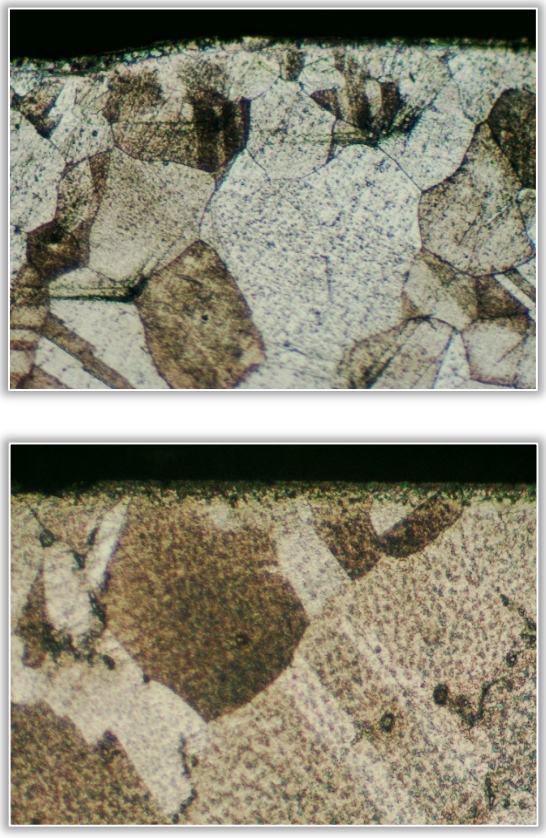

(a) (b)

Plate 2. Optical micrographs of samples oxidized at 1050°C for 4 hours (a) Haynes 282 Sample 1 (100*x*), (b) Inconel 718 Sample A (100*x*)

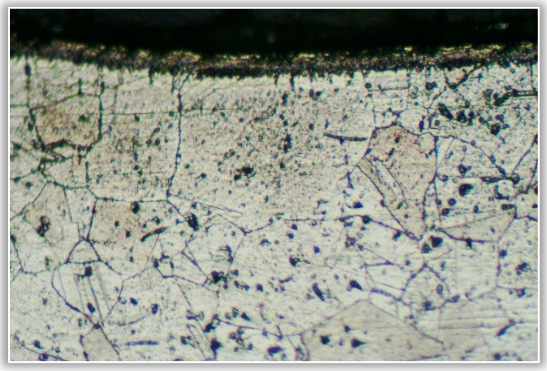

(a)

(b)

Plate 3. Optical micrographs of samples oxidized at 1050°C for 6 hours (a) Haynes 282 Sample 2 (100*x*), (b) Inconel 718 Sample B (100*x*)

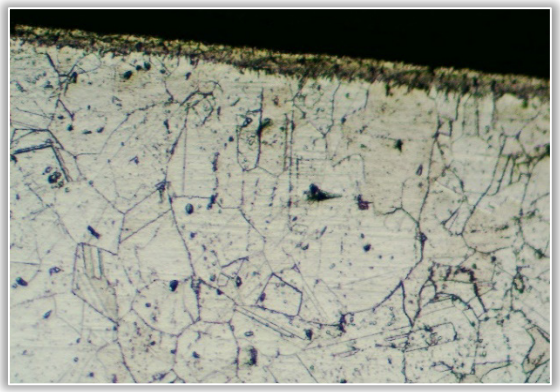

(a)

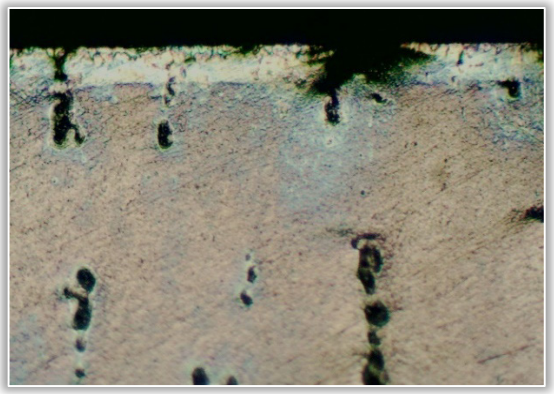

(b)

Plate 4. Optical micrographs of samples oxidized at 1050°C for 8 hours (a) Haynes 282 Sample 3 (100*x*), (b) Inconel 718 Sample C (100*x*)

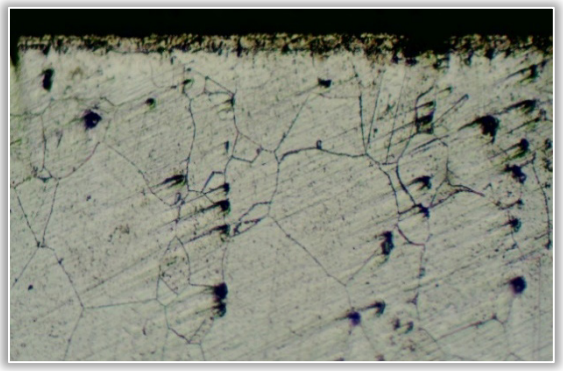

(a)

(b)

Plate 5. Optical micrographs of samples oxidized at 1050°C for 10 hours (a) Haynes 282 Sample 4 (100*x*), (b) Inconel 718 Sample D (100*x*)

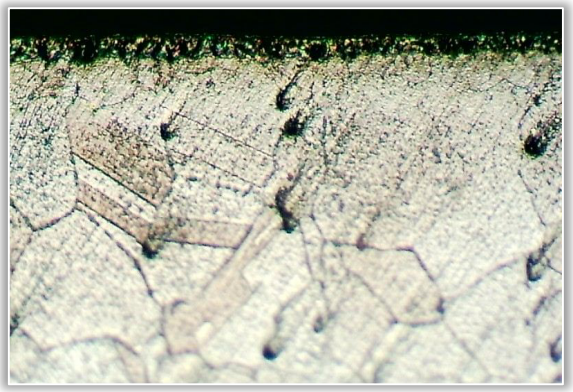

(a)

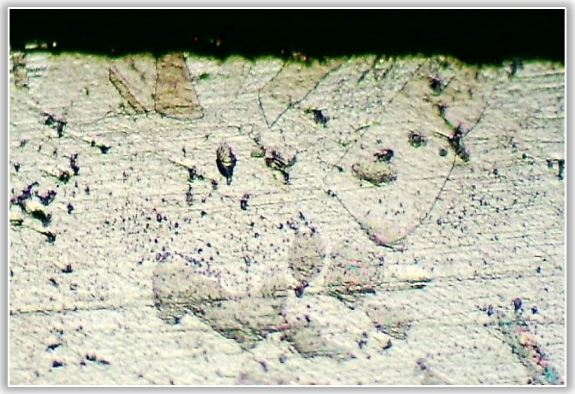

(b)

Plate 6. Optical micrographs of samples oxidized at 1100°C for 4 hours (a) Haynes 282 Sample 5 (100x), (b) Inconel 718 Sample E (100x)

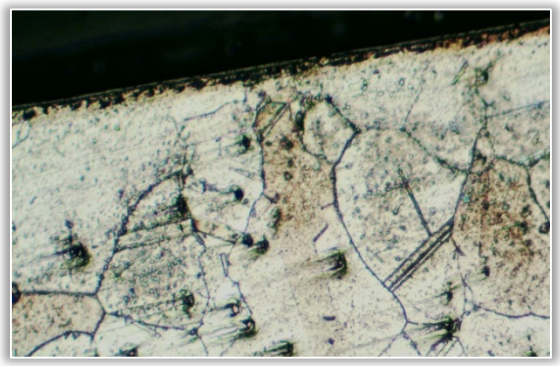

(a)

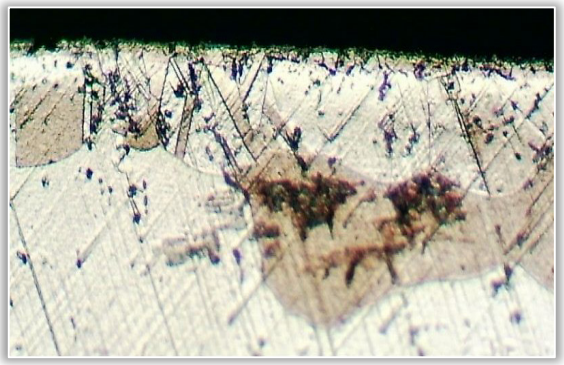

(b)

Plate 7. Optical micrographs of samples oxidized at 1100°C for 6 hours (a) Haynes 282 Sample 6 (100x), (b) Inconel 718 Sample F (100x)

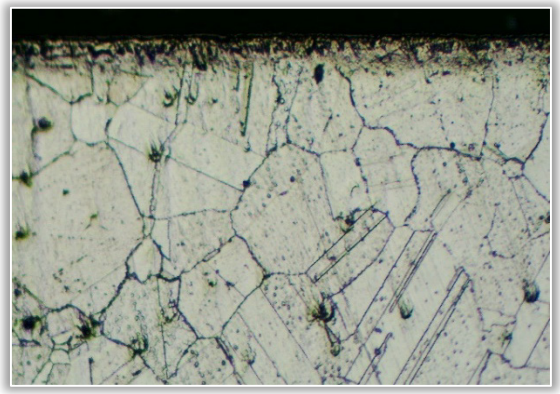

(a)

(b)

Plate 8. Optical micrographs of samples oxidized at 1100°C for 8 hours (a) Haynes 282 Sample 7 (100*x*), (b) Inconel 718 Sample G (100*x*)

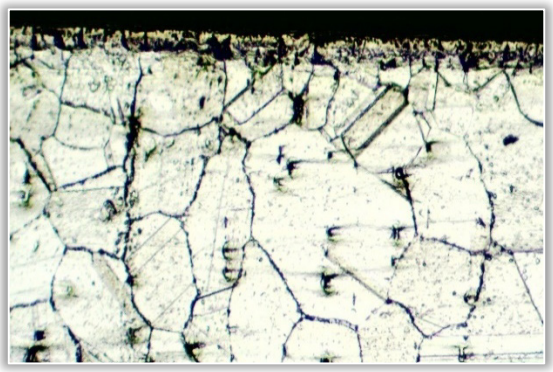

(a)

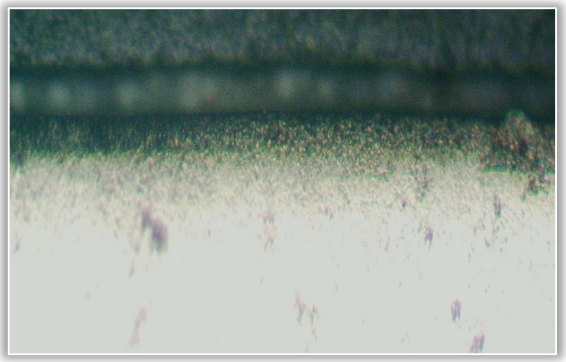

(b)

Plate 9. Optical micrographs of samples oxidized at 1100°C for 10 hours (a) Haynes 282 Sample 8 (100*x*), (b) Inconel 718 Sample H (100*x*)

All examined cross sections of both superalloys' oxidized samples showed distinctly oxidized regions at the top exposed surfaces. However, the thickness of the formed–oxide film was not readily determinable from the light optical microscope used. This could have been due to software limitations. Therefore, measurement of the oxide layer thickness in this present study was not performed using light optical microscopy to prevent inconsistency of results in oxide thickness determination.

SEM and EDS Analyses

In order to characterize the oxide morphology, the top surfaces of oxidized samples were examined using SEM. Elemental composition of the formed–surface–oxides was analysed using EDS. For this investigation, the Phenom Desktop SEM machine with Phenom ProX software attached, in Covenant University, Ota, Ogun State, Nigeria was used.

Oxidized Haynes 282 superalloy

Figures 4 and 5 show the external surface SEM image and spot EDS analysis of Haynes 282 samples oxidized at 1050 and 1100°C for 10 hours.

Oxidized Inconel 718 superalloy

Figures 6 and 7 show the external surface SEM image and spot EDS analysis of Inconel 718 samples oxidized at 1050 and 1100°C for 10 hours each.

SEM surface oxide morphologies of Inconel 718 samples oxidized for 10 hours at 1050 and 1100°C, as observed show cluster–like oxide structures. EDS elemental composition at both test temperatures as observed, was predominantly Cr, and O; suggesting presence of a chromium oxide film.

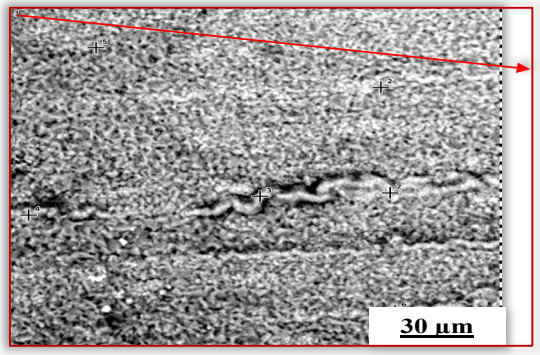

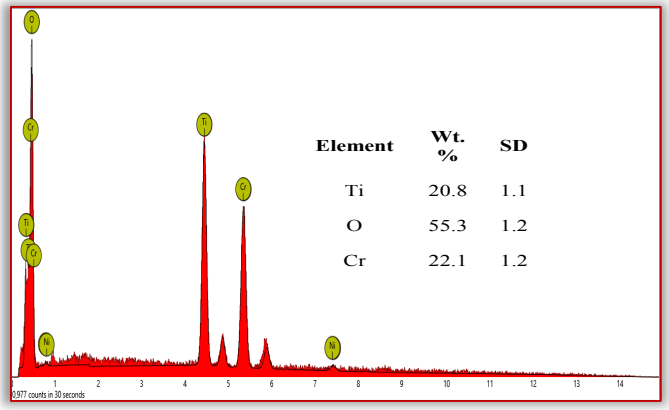

Figure 4. External surface SEM image of Haynes 282 sample oxidized at 1050°C for 10 hours (2,500*x*) with EDS spectrum of spot 1 attached

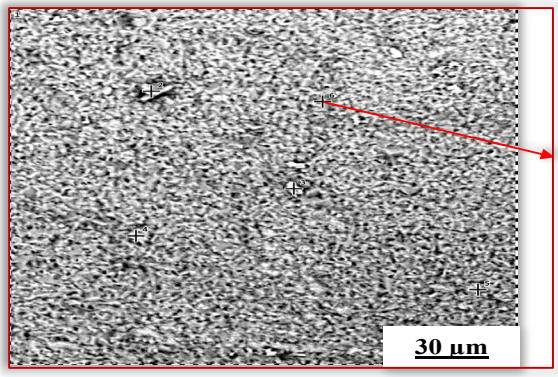

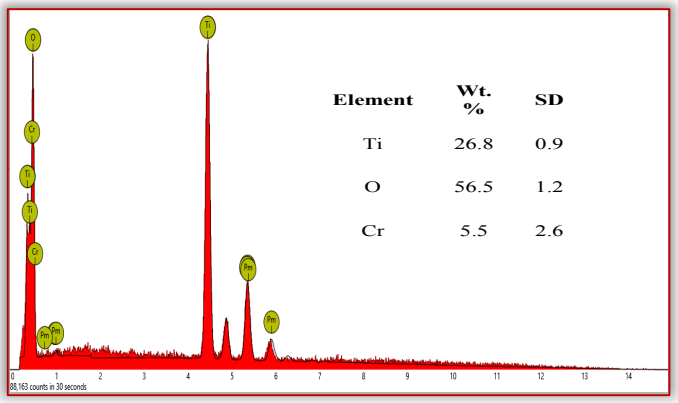

Figure 5. External surface SEM image of Haynes 282 sample oxidized at 1100°C for 10 hours (2500*x*) with EDS spectrum of spot 6 attached.

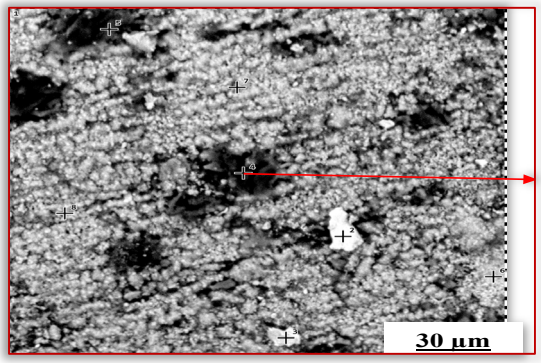

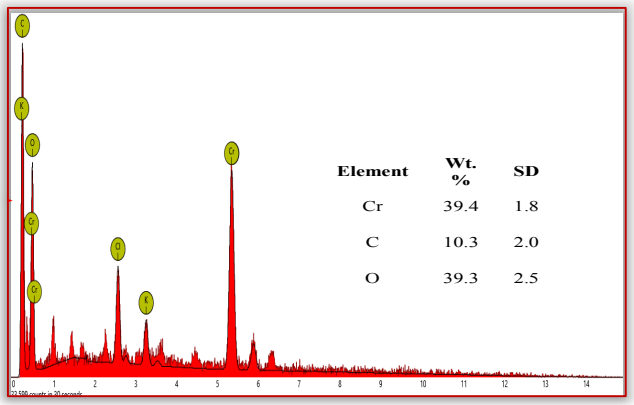

Figure 6. External surface SEM image of Inconel 718 sample oxidized at 1050°C for 10 hours (2,500*x*) with EDS spectrum of spot 4 attached

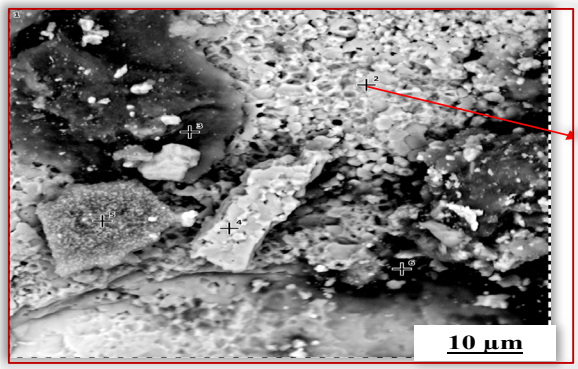

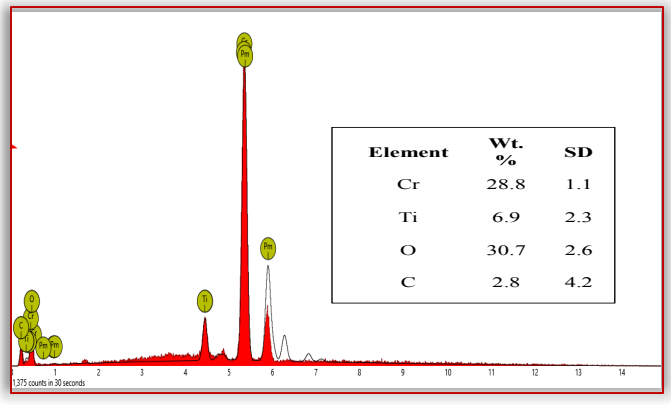

Figure 7: External surface SEM image of Inconel 718 sample oxidized at 1100°C for 10 hours (5000*x*) with EDS spectrum of spot 2 attached

DISCUSSIONS

Oxidation resistance of superalloys is fundamentally due to the formation of adherent oxide layers. These oxides are formed by a selective oxidation of the elements in the alloy, which is affected by a number of factors including relative concentration of reactive elements, cracking behaviour of the oxide scale, and an upper–temperature limit for oxide failure (Pérez–González et al., 2014; Smith, 2013).

Typically, nickel–based superalloy gas turbine components form protective oxides such as Cr_2O_3 (chromia) when exposed to oxidizing environments at high temperatures. Often, the rate of formation of chromium oxides is quicker in comparison with other protective oxides. This makes chromium oxide a preferred oxide since it will form quickly to protect the alloy, and will repair itself quickly in the event of oxide layer spallation. However, chromium oxide may lose its protective properties at temperatures above 1000**℃**, leading to formation of volatile CrO_3. Consequently, Cr_2O_3 alone may not provide sufficient oxidation protection at very high temperatures (Cottis et al., 2010; Smith, 2013)

CONCLUSIONS

This study has shown that:

- At temperatures of 1050 and 1100°C, a thin protective oxide film was developed on the surfaces of both Inconel 718 and Haynes 282 superalloys.
- Haynes 282 has significantly higher isothermal oxidation rate, kp than Inconel at 1050°C but a slightly higher kp than Inconel at 1100°C.
- At both temperatures the elemental composition of the oxide film observed on Haynes 282 suggested presence of chromium oxide containing some titanium oxide–film at both temperatures, while elemental composition of Inconel 718 suggested presence of chromium oxide.

Acknowledgements

Test materials for this work were received through the kind assistance of Prof. A. O. Ojo of the department of Mechanical and Production Engineering, University of Manitoba, Canada. Special thanks to the Management of MIDWAL ENGINEERING (Metallurgical Engineers and Testing Laboratory), Lekki, Lagos, Nigeria.

References

[1] Ahlatci, H. (1991). The use of coatings for hot corrosion and Erosion protection in turbine hot section components. Journal of Engineering Sciences, 5(1), 885–892.
[2] ASM International, ASM Metals Handbook Special Volume: Heat Resistant Materials. ASM International, 1997.
[3] Barbosa, C., Nascimento, J. L., Caminha, I.M. V., and Abud, I. C. (2005). Microstructural aspects of the failure analysis of nickel base superalloys components. Elsevier, Engineering Failure Analysis, 12, 348–361.
[4] Caron, P. and Khan, T. (1999). Evolution of Ni–based superalloys for single crystal gas turbine blade applications. Aerospace Science Technology, 3, 513–523.
[5] Eliaz, N., Shemesh, G. and Latanision, R. M. (2002). Hot corrosion in gas turbine components. Pergamon, Engineering Failure Analysis, 9, 31–43.
[6] Mahobia, G. S., Sudhakar R.G., Antony, A., Chattopadhyay, K., Srinivas, N. C. S. and Singh, V. (2013). Effect of Salt Coatings on Low Cycle Fatigue Behavior of Nickel–base Superalloy GTM–SU–718. Elsevier, Procedia Engineering, 55, 830–834.
[7] Olivares, R. I., Stein, W., and Marvig, P. (2013). Thermogravimetric study of oxidation–resistant alloys for high–temperature solar receivers. Journal of The Minerals, Metals & Materials Society (JOM–TMS), 65(12), 1660–1669.
[8] Pérez–González, F. A., Garza–Montes–de Oca, N. F., Colás, R. (2014). High Temperature Oxidation of the Haynes 282 Nickel–based Superalloy. Springer, Oxidation of Metals, 82, 145–161.
[9] Pollock, T M. and Tin, S. (2006). Nickel–based superalloys for advanced turbine engines: Chemistry, microstructure and properties. Journal of Propulsion and Power, 22(2), 361–374.
[10] Pomeroy, M. J. (2005). Coatings for gas turbine materials and long–term stability issues," Materials and Design, 26(3), 223–231.
[11] Saravanamutto, H., Rogers, G., Cohen, H., and Straznicky, P. (2009). Gas Turbine Theory, Sixth Edition ed. Edinburgh Gate, Harlow, England: Pearson Education Limited.
[12] Shukla, V. N., Jayaganthan, R., and Tewari, V. K. (2013). Oxidation and Hot Corrosion Behaviour of Ni–based Superalloy Inconel 718 in Na2SO4–75%V2O5 Environment at Elevated Temperature. International Journal of Surface Engineering & Materials Technology, 3(1), 20–24. ISSN: 2249–7250.
[13] Sinharoy, S. and Narasimhan, S. L. (2004). Oxidation behaviour of two nickel–base superalloys used as elevated temperature valves in spark ignited engines and diesel exhaust recirculation (EGR) applications. Superalloys 2004, Edited by K. A. Green, T. M. Pollock, H.
[14] Harada, T. E. Howson, R. C. Reed, J. J. Schirra, and S. Walston. TMS (The Minerals, Metals & Materials Society), 623–626.
[15] Smith, M. M. (2013). Comparative Oxidation Study of Un–coated and coated CMSX–4 and CMSX–486 Single Crystal Superalloys. Masters' Thesis, University of Manitoba, Winnipeg, Canada.
[16] The University of Manchester, Shreir's Corrosion, 4th ed., R. A. Cottis et al., Eds. Amsterdam, Netherlands: Elsevier Ltd., 2010, Vol. 1.
[17] Wu, Y., Li, X. W., Song, G. M., Wang, Y. M., and Narita, T. (2010). Improvement of the oxidation resistance of the single–crystal Ni–based TMS–82+ superalloy by Ni–Al coatings with/without the diffusion barrier. Springer, Oxidation of Metals, 74, 287–303. DOI 10.1007/s11085–010–9211–9.
[18] Zitnansky, M., Zrník, J., Martinkovic, M. (1998). Developing processes of property improvement of nickel base superalloys. Elsevier, Journal of Materials Processing Technology, 78, 204209

ISSN: 2067-3809